Impedance Matrix Compression (IMC) Using Iteratively Selected Wavelet Basis

Zachi Baharav, *Student Member, IEEE*, and Yehuda Leviatan, *Fellow, IEEE*

***Abstract*— In this paper, we present a novel approach for the incorporation of wavelets into the solution of frequency-domain integral equations arising in scattering problems. In this approach, we utilize the fact that when the basis functions used are wavelet-type functions, only a few terms in a series expansion are needed to represent the unknown quantity. To determine these dominant expansion functions, an iterative procedure is devised. The new approach combined with the iterative procedure yields a new algorithm that has many advantages over the presently used methods for incorporating wavelets. Numerical results which illustrate the approach are presented for three scattering problems.**

***Index Terms*—Electromagnetic scattering, wavelet transforms.**

I. Introduction

WAVELET expansions have been employed recently in numerical solutions of commonly used frequency-domain integral equations [1]–[5]. In the conventional approach to the solution of these integral equations [1], the unknown quantity of interest (usually the current on the scatterer) is first expanded in terms of a set of wavelet basis functions. Then the difference between the two sides of the equation is forced to be orthogonal to a set of wavelet testing functions. This amounts to describing the operator, which is a convolution integral of the unknown quantity with the Green's function, in a wavelet basis. In many cases, the wavelet testing functions are nearly orthogonal to the fields due to the wavelet basis functions. Hence, the resultant matrix representation of the operator (the impedance matrix) is highly localized and it becomes diagonally dominant as the wavelet functions get spatially narrower. In these cases, the impedance matrix can undergo a thresholding operation, which renders the matrix sparse. However, this virtue of being localized is liable to be scatterer geometry dependent. Moreover, once thresholding has been applied there is no systematic way (other than trivially using smaller threshold levels) leading to a more accurate solution.

In this paper, a different approach is proposed. Rather than resorting to the sparseness of the operator in the wavelet expansion, we utilize the sparse representation of the (yet unknown) quantity in the wavelet expansion. It is well known that wavelets can represent nonstationary signals with only a few terms; namely, when one expands such a signal in a wavelet series, only few terms are dominant and constitute the major part of the signal energy. This fact has mainly been applied for compression purposes in signal processing [6]–[8], but recently it has also been used in computational electromagnetics [9], [10]. In [9], [10], instead of solving for all the coefficients in the wavelet expansion of the unknown induced current, only those expected to be dominant based on the physical optics approximation of the current have been solved for.

In this paper, the determination of the dominant coefficients is affected systematically using an iterative procedure. The iterative procedure allows to zoom in on the fine details of the signal in any region of interest. It also provides a means for gradually attaining higher accuracy level. The matrices involved are much smaller and, hence, the solution requires significantly less memory and run time. Clearly, the subset of basis functions providing good approximation to the current on the scatterer for a certain excitation may not be best suited for other excitations. Hence, the iterative basis selection procedure should be repeated over again each time the incident field changes.

The organization of the paper is as follows. In the next section, the problem under study is specified and formulated using a wavelet expansion. Section III embodies the description of the iterative compression algorithm, comprising an iterative wavelet basis selection that is followed by a matrix compression (as opposed to thresholding) procedure. Numerical results are described in Section IV. Finally, summary and conclusions are given in Section V.

II. Formulation

Without loss of generality, let us consider the scalar problem of computing the current J_z on the perimeter of a perfectly conducting z-directed cylinder excited by a TM_z wave, as described in Fig. 2. This scattering problem can be formulated in various ways, but here we resort to the E-field integral equation formulation. To overcome the difficulties associated with the integration of the wavelet functions, N conventional pulse-basis functions are used initially to expand the current. We have

$$J_z = \sum_{i=1}^{N} I_i P_i \tag{1}$$

where P_i denotes the pulse-function centered about the ith source point on the cylinder perimeter and I_i is the yet

Manuscript received December 4, 1995; revised October 31, 1996. This work was supported in part by the Fund for the Promotion of Research at the Technion.

The authors are with the Department of Electrical Engineering, Technion—Israel Institute of Technology, Haifa, 32000 Israel.

Publisher Item Identifier S 0018-926X(98)01491-4.

unknown coefficient of the pulse-function P_i. Applying the E-field integral equation in the least-square error sense at M testing points on the cylinder perimeter ($M \geq N$), we arrive formally at

$$[Z]\vec{I} = \vec{V} \tag{2}$$

where $[Z]$ is the impedance matrix, $\vec{I}$ is the (unknown) current vector, and $\vec{V}$ is the excitation vector.

In order to transform the pulse basis functions into wavelet basis functions, we introduce an $N \times N$ transformation matrix $[T_I]$ (which is assumed to be real and unitary) and denote the transpose of $[T_I]$ by $[\tilde{T}_I]$. The rows of $[T_I]$ describe the new wavelet basis functions in terms of the pulses. Similarly, to transform the individual testing points into wavelet testing arrays, we introduce an $M \times M$ transformation matrix $[T_V]$, which is assumed to be real and unitary. The rows of $[T_V]$ describe the new wavelet testing arrays in terms of the individual testing points. The basis transformations are now effected by

$$\vec{A} = [T_I]\vec{I} \tag{3}$$

$$\vec{B} = [T_V]\vec{V} \tag{4}$$

$$[\mathcal{Z}] = [T_V][Z][\tilde{T}_I] \tag{5}$$

and we arrive at the matrix equation

$$[\mathcal{Z}]\vec{A} = \vec{B}. \tag{6}$$

This matrix equation is equivalent (in terms of the resulting J_z) to the previous matrix equation given by (2). However, in (6), both the source functions and testing points are expressed in the respective wavelet bases. Thus, the current J_z can be expressed as

$$J_z = \sum_{i=1}^{N} A_i W_i \tag{7}$$

where $\{W_i\}$, $i = 1, 2, \cdots, N$ denote the wavelet functions and $\{A_i\}$, $i = 1, 2, \cdots, N$ are the elements of $\vec{A}$.

III. Iterative Compression Algorithm

In this section, rather than solving (6) or a thresholded version of this matrix equation for $A_1, \cdots, A_N$ [which determine J_z by (7)], we apply an iterative algorithm for the selection of the dominant wavelet basis functions. The iterative algorithm facilitates a systematic determination of the more significant terms in the series expansion (7) and thereby allows a solution of a much smaller matrix equation for the evaluation of J_z. Clearly, the iterative algorithm can be carried on toward using all the basis functions to yield the very same solution as that of the original matrix (2). However, our intent is to derive an accurate enough solution for (2) while using a significantly smaller number of basis functions.

A. Algorithm Description

The iterative compression algorithm is depicted as a flow chart in Fig. 1. The steps of the algorithm are described below.

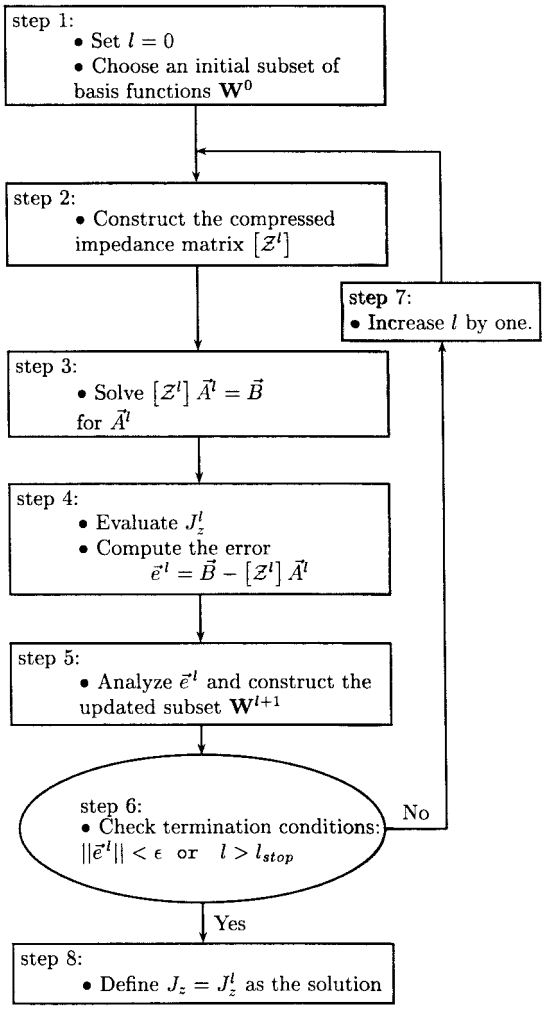

Fig. 1. Iterative compression algorithm. The various steps are described in some more detail in the text (see Section III-A).

Step 1—Initialization: Let l denote a typical iteration and let the subset $\mathbf{W}^l = \{W_{i(k)}\}_{k=1}^{N_l}$ consisting of N_l basis functions be the associated iterate. Set l to zero and choose the initial iterate $\mathbf{W}^0$. This iterate comprises a small number N_0 of wavelet functions $\{W_{i(k)}\}_{k=1}^{N_0}$ taken as a crude approximation for the basis needed for expanding the unknown current J_z. In the examples that follow we use $N_0 = 1$ since it is generally a good practice to take N_0 as small as possible and let the algorithm select iteratively the relevant basis functions. However, if a good estimate of the unknown current is available, one might consider starting out with a larger set of appropriate basis functions.

Step 2—Impedance Matrix Compression: Consider the subset of basis functions $\mathbf{W}^l = \{W_{i(k)}\}_{k=1}^{N_l}$ along with the corresponding subset of unknown coefficients $\{A_{i(k)}\}_{k=1}^{N_l}$. Cast the coefficients $\{A_{i(k)}\}_{k=1}^{N_l}$ into a column vector $\vec{A}^l$ and construct a matrix $[\mathcal{Z}^l]$, comprising the $\{i(k)\}_{k=1}^{N_l}$ columns of the impedance matrix $[\mathcal{Z}]$.

Step 3—Determination of $\vec{A}^{\,l}$: Solve $[\mathcal{Z}^l]\vec{A}^{\,l} = \vec{B}$ for the vector of coefficients $\vec{A}^{\,l}$. The dimensions of $[\mathcal{Z}^l]$, $\vec{A}^{\,l}$, and $\vec{B}$ are $M \times N_l$, $N_l \times 1$, and $M \times 1$, respectively.

Step 4—Error Computation: Once $\vec{A}^{\,l}$ is known, the current J_z may be approximated by

$$J_z^l = \sum_{k=1}^{N_l} A_{i(k)} W_{i(k)}. \tag{8}$$

The field due to J_z^l does not produce the exact scattered field. Hence, the required boundary condition is not satisfied. This fact manifests itself as an error in satisfying (6). This error is given by

$$\vec{e}^{\,l} = \vec{B} - [\mathcal{Z}^l]\vec{A}^l. \tag{9}$$

Since the right-hand side of (9) is expressed in terms of wavelet basis functions, so is $\vec{e}^{\,l}$. This implies that the boundary condition error along the perimeter can be expressed as

$$E^l = \sum_{i=1}^{M} e_i^l W_i \tag{10}$$

where $\{e_i^l\}_{i=1}^M$ are the elements of $\vec{e}^{\,l}$.

Step 5—Construct the Updated Subset $\mathbf{W}^{l+1}$*:* Toward reducing the boundary condition error along the perimeter (10), we search for the largest (in terms of magnitude) element of $\vec{e}^{\,l}$. If the basis function associated with this element *is* contained in $\mathbf{W}^l$, we pursue the next largest element of $\vec{e}^{\,l}$. The above search is repeated until we find a preset number of largest elements of $\vec{e}^{\,l}$, whose associated basis functions *are not* in $\mathbf{W}^l$. These basis functions are then added to $\mathbf{W}^l$ to form an updated subset $\mathbf{W}^{l+1}$.

The idea is to deduce information as to which basis functions will allow a more compact, yet accurate, representation of the current from the error coefficient vector. The idea is based on the apparent correlation between the wavelet expansion of the error and the wavelet expansion of the unknown current. This correlation is even more profound when we deal with the rapidly varying parts of the error. The rapidly varying parts are associated with wavelet expansion functions that are spatially narrow and characterized by high spatial-frequency content. Such wavelet functions radiate quite poorly and their fields are, therefore, highly localized. Hence, by adding these functions to the set used for spanning the current, one can affect the error locally.

Step 6—Check Stopping Criteria: Two stopping rules are checked. If either the norm of the error is smaller then a predefined value ϵ or the iteration count has exceeded a predefined number l_{stop} the iterative process terminates and we proceed directly to Step 8. Otherwise, the iterative process continues to the next step.

Step 7—Prepare for Next Iteration: The iteration counter is increased by one and we move on to begin a new iteration (Step 2).

Step 8—Evaluation of J_z*:* This is the final step. An approximation for the unknown current J_z can be obtained from (8). We have

$$J_z = J_z^l. \tag{11}$$

B. Implementation Remarks

In the previous section, we have described the algorithm in a somewhat concise manner. Following are a few issues which are important for a successful implementation of the algorithm.

First, one should note that the computational burden involved in the solution of the matrix equation in Step 3 can be lessened by applying a conventional thresholding procedure to $[\mathcal{Z}^l]$. Since $[\mathcal{Z}^l]$ is not only compressed but also localized, it will be rendered sparse and allow the use of a sparse matrix solver for solving $[\mathcal{Z}^l]\vec{A}^l = \vec{B}$.

A second issue related to Step 3 is the possibility of deducing knowledge from the previous iteration for the solution of the matrix equation in the current one. There are basically two ways to solve the matrix equation. One is by a direct inversion using the pseudo-inverse of $[\mathcal{Z}^l]$ [11, p. 221] and the other is by an iterative solution such as the conjugate-gradient [11, pp. 516–529]. If the direct inversion approach is applied, one can exploit the knowledge of the inverse of $[\mathcal{Z}^{l-1}]$ since $[\mathcal{Z}^{l-1}]$ is a submatrix of $[\mathcal{Z}^l]$. If an iterative solution is applied, one can choose the vector $\vec{A}^{l-1}$ as the initial guess for the solution. Since this guess is presumably close to the solution $\vec{A}^l$, the iterative solution will converge faster.

The last issue concerns the compression of the impedance matrix. As described in the algorithm (Steps 2 and 3), we first construct the compressed impedance matrix $[\mathcal{Z}^l]$ and, in turn, solve $[\mathcal{Z}^l]\vec{A}^l = \vec{B}$ for the vector of unknown coefficients $\vec{A}^l$ in the least-squares error sense. However, the determination of $\vec{A}^l$ in Step 3 can also be effected by solving $[Z][T_I]\vec{A}^l = \vec{V}$ in the least-squares error sense. Clearly, these two matrix equations are equivalent as far as $\vec{A}^l$ is concerned. Yet, the latter one can be row reduced in a rather straightforward manner and solved for an approximate $\vec{A}^l$ in a faster way. Hence, it is naturally preferred. The thinning of the rows is done while ensuring that the testing points corresponding to the rows retained are equally distributed along the circumference of the scatterer and it involves the following tradeoff: on one hand, as more rows are omitted (as long as at least N_l rows are kept), the solution becomes less computationally intensive. On the other hand, solving an overdetermined set of equations offers stability by rendering the solution less sensitive to the exact location of test points. Based on our experience, keeping the number of rows three times the number of unknowns strikes a via media between efficiency and stability. Once the approximation of $\vec{A}^l$ is found, the error in satisfying (6), which is given in Step 4 by (9), is obtained by

$$\vec{e}^{\,l} = [\tilde{T_V}](\vec{V} - [Z][T_I]\vec{A}^l). \tag{12}$$

IV. Numerical Results

In this section, we consider three scattering problems. Representative computations are given to show how the iterative compression algorithm operates and to demonstrate its merits.

The first problem analyzed is that of a TM_z plane wave scattering by a perfectly conducting circular cylinder. The geometry of this scattering problem is depicted in Fig. 2. The

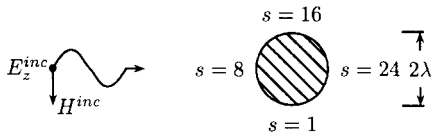

Fig. 2. Scattering problem of a circular conducting cylinder excited by a TM_z incident plane wave. The length parameter along the perimeter is denoted by s.

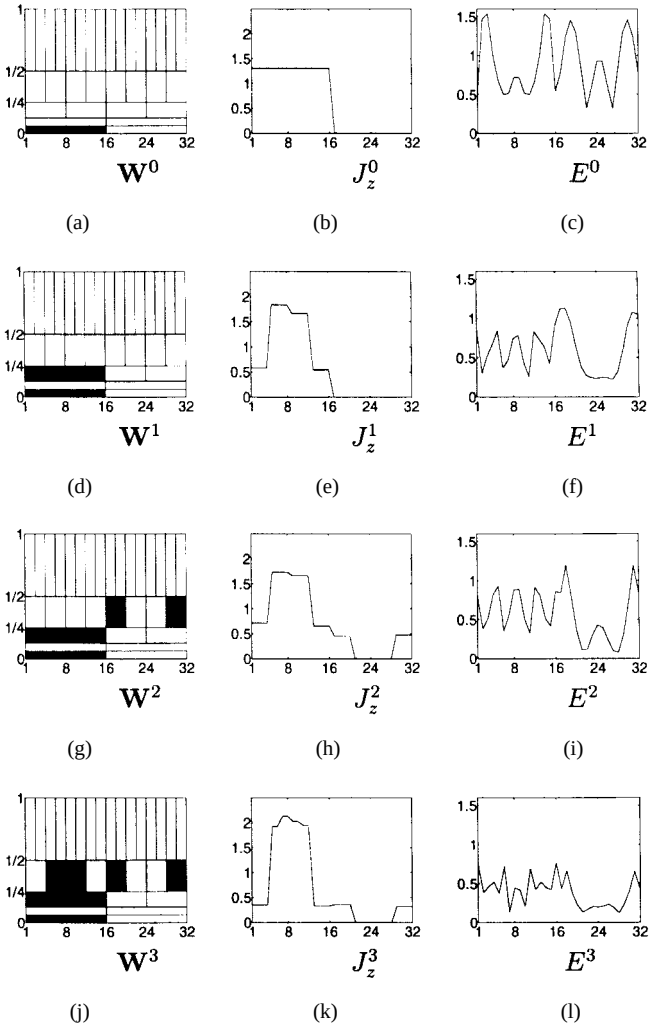

Fig. 3. Results obtained in the first four iterations of the iterative solution for the scattering problem depicted in Fig. 2.

incident wave is of unit magnetic field. The radius of the cylinder is equal to one wavelength. The circular perimeter has been divided into 32 equally spaced pulses, which were, in turn, transformed into a Haar wavelet basis. The Haar basis, while very simple, is just right for conveying the main ideas of the paper. It is quite possible though that the use of smoother wavelets would have yielded more accurate results with fewer basis function. The longest wavelet basis function is comprised of 16 pulses and covers half of the cylinder circumference. Results obtained in each of the first 11 iterations are depicted in Figs. 3 and 4. The results obtained in each iteration are divided into three data sets, which are represented separately in three different figures:

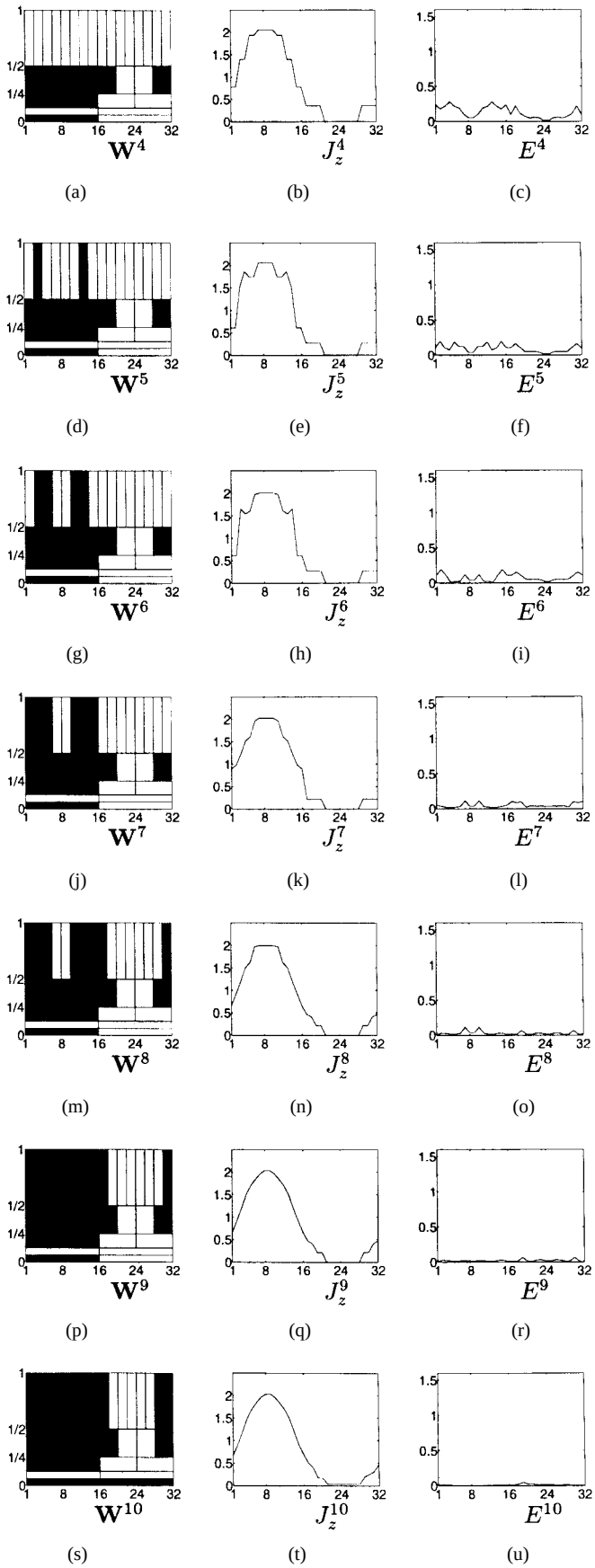

Fig. 4. Results obtained in iterations 4–10 of the iterative solution for the scattering problem depicted in Fig. 2.

- The figures situated on the left (denoted (a), (d), (g), $\cdots$) display on a combined-space grid the pertinent set $\mathbf{W}^l$ of wavelet basis functions. The basis functions involved are denoted by black rectangles. The horizontal axis in these figures is the spatial location and the vertical axis describes the spatial variation (for a detailed discussion of such representations of the combined space see, for example, [12], [13]). Note that there are 32 rectangles corresponding to the 32 wavelet basis functions used, partitioning the combined space. The two rectangles at the bottom [one of them is colored black in (a)] correspond to the two basis functions that, for the Haar basis, are constant over half of the cylinder circumference. The left half of these drawings pertains to wavelet functions that are in the the lit region. The upper part corresponds to wavelet functions suitable for describing the rapid spatial variations of the current.
- The figures situated in the center (denoted (b), (e), (h), $\cdots$) describe the magnitude of the approximate current J_z^l as evaluated in each iteration via (8). The currents are given in values which are normalized to the magnitude of the incident magnetic field. These figures demonstrate best the progressive improvement of the approximation for the current J_z achieved with this iterative scheme.
- The figures situated on the right (denoted (c), (f), (i), $\cdots$) describe the magnitude of the error in satisfying the boundary condition $\vec{E}^l$ as evaluated in Step 4 of each iteration by (10). The field-errors are given in values, which are normalized to the magnitude of the incident electric field.

Let us now review the iterative scheme in somewhat more detail. Fig. 3(a) describes the initial set $\mathbf{W}^0$ employed. Here, we start with only one basis function, which is of constant amplitude over half of the cylinder (in the lit region). This basis function is denoted by a black rectangle in (a). Fig. 3(b) shows the approximation obtained after solving for the coefficient of the basis function described in (a). The error in satisfying the boundary condition is displayed in Fig. 3(c). The wavelet series coefficients of this error are evaluated and this information is analyzed to determine two additional basis functions which together with the initial set $\mathbf{W}^0$ form the updated set $\mathbf{W}^1$ shown in Fig. 3(d). Similar explanation can be extended to the rest of the figures. It is interesting to note that due to the symmetry of the problem the basis functions are chosen symmetrically as well. This is effected *without* any outside intervention and is due to the fact that the symmetry of the geometry and the excitation is reflected in the error vector. Fig. 3 describes the first four iterations and the next seven iterations are described in Fig. 4. The last iteration shown is the tenth iteration, which involves 21 basis functions. A reference solution is depicted for comparison in Fig. 5. The reference solution is the one arrived at iteration 15 and which involves 31 basis functions.

The second example considers the scattering of a TM_z plane wave by a perfectly conducting cylinder of square cross section. The geometry of this scattering problem is depicted in Fig. 6. The scatterer perimeter is divided in this case into 64 equally spaced pulses and, as before, a Haar wavelet basis is used. The longest wavelet basis function consists of 16 pulses and covers one side of the cylinder. Shown in Fig. 7 are results obtained in progressive numbers of iterations, describing how the approximate current gradually approaches the correct one. Note that after iteration 7 there is an error in satisfying the boundary condition in the vicinity of the upper left edge of the cylinder $(s = 16)$. Projecting this error on the wavelet basis, a spatially narrow wavelet function is automatically selected, which, in the subsequent iteration (iteration 8), adequately represents the singularity of the current distribution near the upper left edge.

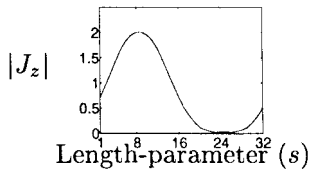

Fig. 5. Magnitude of current density J_z along the circular perimeter of the scatterer for the scattering problem illustrated in Fig. 2, obtained with 31 basis functions.

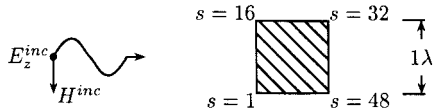

Fig. 6. Scattering problem of a conducting cylinder of square cross section excited by a TM_z incident plane wave. The length parameter along the perimeter is denoted by s.

Now we turn to a brief comparison between the new approach and the conventional one where the impedance matrix undergoes thresholding, which renders the matrix sparse. Comprehensive comparison between the thresholding method and impedance matrix compression method can be found in [9] and [10]. Fig. 8 describes the performance of the two algorithms. The vertical axis describes ΔE_{bc}, the square of the L_2 norm of the error in satisfying the boundary condition. The horizontal axis is the compression ratio. The compression ratio is equal to one minus the ratio between the number of nonzero elements of $[\mathcal{Z}^l]$ in the last iteration performed and the number of elements of the original matrix. Note that while we consider the matrix $[\mathcal{Z}^l]$ in the last iteration as a measure of complexity, one must recall that other matrix equations, albeit smaller in size, have been solved in the preceding iterations. The advantage of the new algorithm is clearly seen in the figure. Another perspective on the difference between the methods can be gained from Fig. 9. The approximate current obtained based on the thresholding procedure is shown in Fig. 9(a), while the one obtained based on the new algorithm is shown in Fig. 9(b). The fields due to these currents satisfy the boundary condition to within the same average error level of $\Delta E_{\mathrm{bc}} = 0.1\%$. It is seen that the current shown in Fig. 9(a) has many rapidly varying ripples. The wiggly behavior of the solution stems from the fact that all the rapidly varying wavelets are actually playing a part in the solution. In contrast, only part of these wavelets are used to construct the solution shown in Fig. 9(b) and, hence, this solution is smoother.

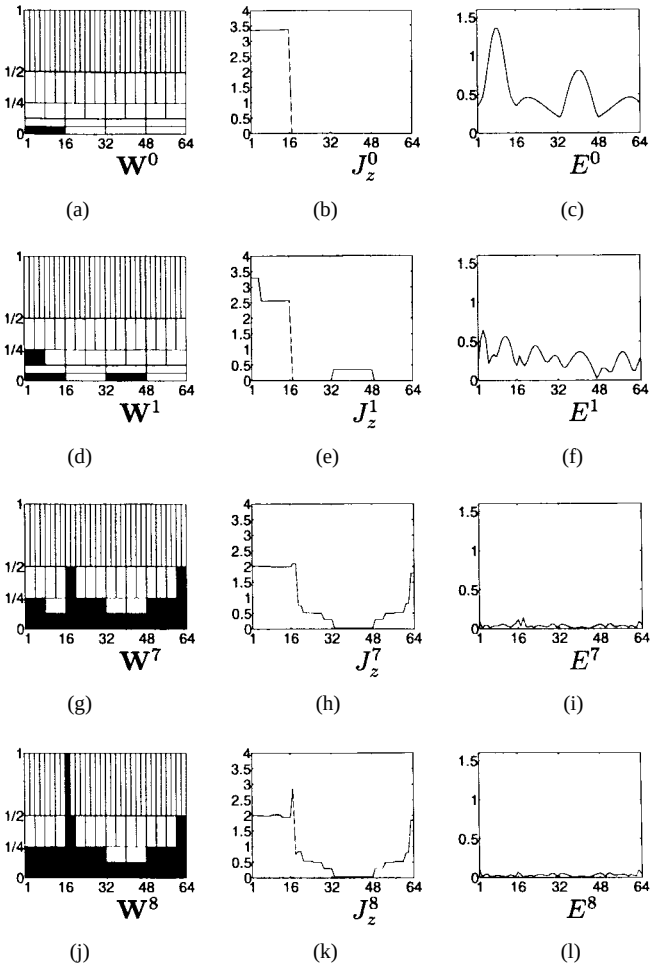

Fig. 7. Results obtained in iterations 0, 1, 7, and 8 of the iterative solution for the scattering problem depicted in Fig. 6.

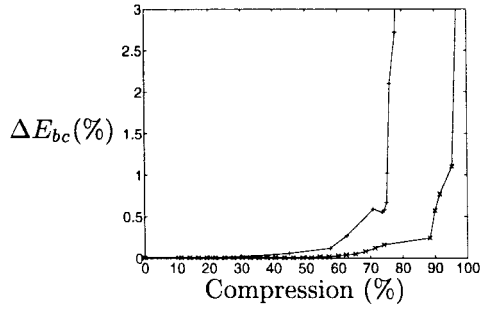

Fig. 8. Boundary condition error versus compression of the impedance matrix for the scattering problem illustrated in Fig. 6, obtained by two solution methods. Cases considered are for the conventional approach of thresholding the original impedance matrix (denoted by pluses) and for the iterative compression algorithm proposed in this paper (denoted by crosses).

We will further exploit the above example to illustrate some of the computational merits of the new method. In this case, a total of 64 pulse-basis functions were originally used to expand the unknown current and the boundary condition was imposed in the least-square error sense at 128 testing points. Thus, if one had pursued the solution using a standard method of moments approach, the size of the resultant impedance matrix would have been 128 $\times$ 64, that is a matrix comprising 8192 complex entries. Moreover, the elements of this matrix would

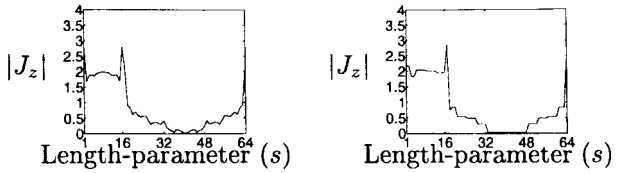

Fig. 9. Magnitude of current density J_z along the perimeter of the square scatterer (depicted in Fig. 6) obtained by two solution methods: cases considered are for (a) the conventional method of thresholding the impedance matrix and (b) the iterative compression algorithm proposed in this paper (at iteration 9). Both solutions are subject to the same accuracy requirements in terms of satisfying the boundary condition.

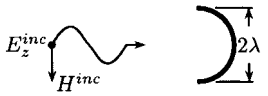

Fig. 10. Scattering problem of a conducting half circular shell excited by a TM_z incident plane wave.

have been comparable in magnitude, which implies that a substantial reduction in the number of matrix elements would not be achieved by means of a thresholding procedure without suffering loss of accuracy. If instead of the pulse functions, Haar wavelets are used to expand the unknown current and Haar wavelet transform is applied to the testing points, the resultant matrix will also comprise 8192 complex entries, but the matrix will be more localized and a thresholding procedure can render the matrix sparse without much degrading solution accuracy. For example, applying a thresholding while allowing an average error level of $\Delta E_{\mathrm{bc}} = 0.1\%$ resulted in 4712 zero elements, which implies a sparseness level of $\frac{4712}{8192} = 0.5752$. Thus, the complexity here is that of solving a 128 $\times$ 64 sparse matrix with 3480 nonzero elements. Finally, to arrive at the same error level of 0.1% using the new compression algorithm, only eight iterations were performed, which resulted in 17 basis functions. As mentioned before, the number of testing points can be reduced proportionately to the reduction in the number of elements. In this example, the number of testing points is approximately three times the number of basis functions. It follows that the matrix arrived at in this case is of size 64 $\times$ 17, that is a matrix of 1088 complex elements, and the compression level is thus

$$\text{Compression} = 1 - \frac{17 \times 64}{64 \times 128} = 0.867. \tag{13}$$

Again, it may be claimed that only the last iteration has been taken into account, but one should keep in mind the fact that the previous iterations involved much smaller matrices and that they could be used as initial guesses for the solution of the matrix equation.

As was mentioned previously, the correlation between the wavelet expansion of the error and wavelet expansion of the current plays a key part in the success of the suggested algorithm, where the error is indicative of which elements should be added to the current expansion. Clearly, it can be argued that in the case of a concave body where the correlation is not as obvious as it is in the case of a convex body, the results will not be as good. The following example

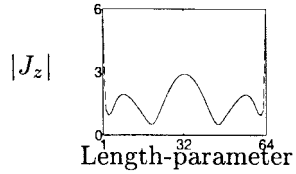

Fig. 11. Magnitude of current density J_z along the circular perimeter of the scatterer for the scattering problem illustrated in Fig. 10, obtained with 64 basis functions.

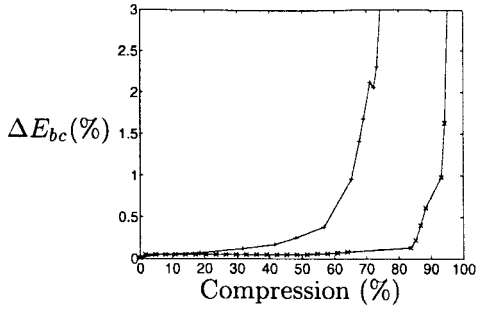

Fig. 12. Boundary condition error versus compression of the impedance matrix for the scattering problem illustrated in Fig. 10, obtained by two solution methods. Cases considered are for the conventional approach of thresholding the original impedance matrix (denoted by pluses) and for the iterative compression algorithm proposed in this paper (denoted by crosses).

thus deals with the scattering by a concave body. The specific configuration considered is that of a half circular shell, as depicted in Fig. 10. The perimeter was divided into 64 pulse-basis functions, which were, in turn, transformed into a Haar wavelet basis. The resultant solution, when neither compression nor thresholding is applied, is shown in Fig. 11. A comparison between the two methods—that of thresholding and that of compression—is given in Fig. 12. It is evident that even in a case where internal reflections exist the iterative basis construction works quite well. This is probably owing to the fact that the correlation between the error and the current in the small scale is conserved regardless of the shape of the scatterer. Finally, Fig. 13 presents intermediate results obtained in the course of the iterative process, which show how the iterative solution for this scattering problem evolves.

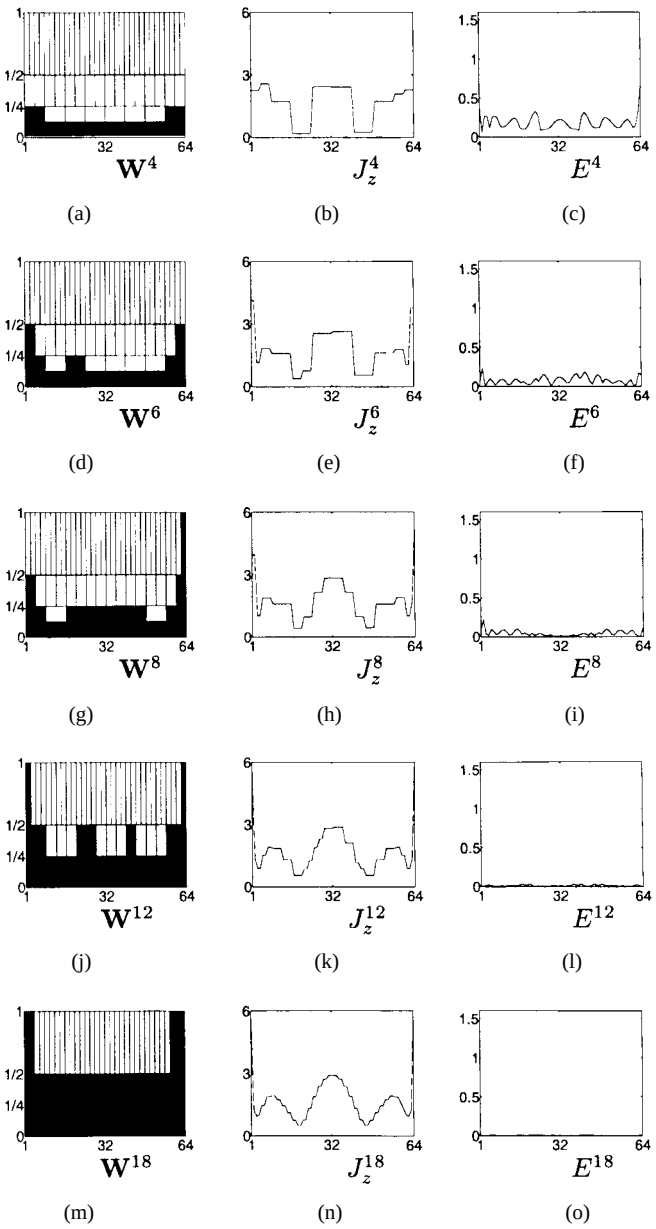

Fig. 13. Results obtained in iterations 4, 6, 8, 12, and 18 of the iterative solution for the scattering problem depicted in Fig. 10.

V. Summary and Conclusions

In this paper, we proposed a new algorithm for the incorporation of wavelets into the solution of integral equations arising in scattering problems. This algorithm utilizes the fact that quite often only a few terms are needed to describe the current on the scatterer to a good approximation. An iterative procedure for the determination of these few terms has been presented. The procedure is based on the apparent correlation between the respective wavelet expansions of the error and the unknown current. Numerical results have been furnished, which demonstrated the applicability and features of the algorithm.

Future research can proceed along two lines. An important continuation can be extension of the approach to more complex problems such as problems involving scattering by metallic and penetrable finite-size bodies. It is quite obvious that many of the ingredients of this two-dimensional solution can be readily generalized to three-dimensional cases. Other efforts can be devoted to dealing exclusively with the iterative algorithm. We believe that by exploring the cases in which the algorithm falls within the class of conjugate directions algorithms [14], one can deduce how the computational efficiency of the algorithm can be improved.

References

[1] B. Z. Steinberg and Y. Leviatan, "On the use of wavelet expansions in the method of moments," *IEEE Trans. Antennas Propagat.*, vol. 41, pp. 610–619, May 1993.

[2] H. Kim and H. Ling, "On the application of fast wavelet transform to the integral-equation solution of electromagnetic scattering problems," *Microwave Opt. Technol. Lett.*, vol. 6, no. 3, pp. 168–173, Mar. 1993.

[3] R. L. Wagner, G. P. Otto, and W. C. Chew, "Fast waveguide mode computation using wavelet-like basis functions," *IEEE Microwave Guided Wave Lett.*, vol. 3, pp. 208–210, July 1993.

[4] B. Z. Steinberg and Y. Leviatan, "Periodic wavelet expansions for analysis of scattering from metallic cylinders," *Microwave Opt. Technol. Lett.*, vol. 7, no. 6, pp. 266–268, Apr. 1994.
[5] J. C. Goswami, A. K. Chan, and C. K. Chui, "An analysis of two-dimensional scattering by metallic cylinders using wavelets on a bounded interval," in *IEEE AP-S Int. Symp. Dig.*, Seattle, WA, June 1994, vol. 1, p. 2.
[6] R. R. Coifman and M. V. Wickerhauser, "Entropy-based algorithms for best basis selection," *IEEE Trans. Inform. Theory*, vol. 38, pp. 713–718, Mar. 1992.
[7] K. Ramchandran and M. Vetterli, "Best wavelet packet bases in a rate-distortion sense," *IEEE Trans. Image Processing*, vol. 2, pp. 160–175, Apr. 1993.
[8] C. H. H. Chu, "Data compression by multiresolution tree search," *Opt. Eng.*, vol. 33, no. 7, pp. 2136–2142, July 1994.
[9] Z. Baharav and Y. Leviatan, "Impedance matrix compression with the use of wavelet expansions," *Microwave Opt. Technol. Lett.*, vol. 12, no. 5, pp. 268–272, Aug. 1996.
[10] ———, "Impedance matrix compression using adaptively constructed basis functions," *IEEE Trans. Antennas Propagat.*, vol. 44, pp. 1231–1238, Sept. 1996.
[11] G. H. Golub and C. F. Van Loan, *Matrix Computations*, 2nd ed. Baltimore, MD: Johns Hopkins Univ. Press, 1989.
[12] C. Herely, J. Kovacevic, R. Ramachandran, and M. Vetterli, "Tilings of the time-frequency plane: Construction of arbitrary orthogonal bases and fast tiling algorithms," *IEEE Trans. Signal Processing*, vol. 41, pp. 3341–3359, Dec. 1993.
[13] I. Daubechies, *Ten Lectures on Wavelets*. Philadelphia, PA: Soc. Indust. Appl. Math., 1992.
[14] J. E. Dennis, Jr. and K. Turner, "Generalized conjugate directions," *Lin. Alg. Applicat.*, vol. 88/89, pp. 187–209, 1987.

Zachi Baharav (S'95), for photograph and biography, see p. 1238 of the September 1996 issue of this TRANSACTIONS.

Yehuda Leviatan (S'81–M'86–SM'88–F'98), for photograph and biography, see p. 1238 of the September 1996 issue of this TRANSACTIONS.